http://ansinet.com/itj

ITJ

ISSN 1812-5638

INFORMATION TECHNOLOGY JOURNAL

ANSInet
Asian Network for Scientific Information
308 Lasani Town, Sargodha Road, Faisalabad - Pakistan

Information Technology Journal 5 (1): 94-107, 2006
ISSN 1812-5638

Evaluation of Standardization of Curve Evolution Based Boundary Mapping Technique for Chromosome Spread Images

[1]A. Prabhu Britto and [2]G. Ravindran
[1]Center for Medical Electronics, Department of Electronics and Communication Engineering,
[2]Faculty of Information and Communication Engineering, Anna University, Chennai 600025, India

Abstract: In this study, the suitability of the characterized parameters governing the DCT based GVF active contour formulation (curve evolution method) as standardized values for boundary mapping chromosome spread images was investigated as an evaluation of standardization of the boundary mapping technique. It was found experimentally that a unique set of parameter values of the technique is required for boundary mapping every chromosome image. Characterization studies showed that each parameter has an optimal range of values within which good boundary mapping results can be obtained for various chromosomes in similar class of images. Statistical testing validates the experimental results of characterization. Standardization of characterized parameters was then carried out using a different dataset comprising of similar class of chromosome spread images so that the standardization testing is independent of dataset.

Key words: Gradient vector flow, active contours, chromosome, boundary mapping, characterization, standardization

INTRODUCTION

This study used characterized Discrete Cosine Transform (DCT) based Gradient Vector Flow (GVF) active contours[1] to assess the standardization of characterized parameters for boundary mapping of chromosome spread images independent of dataset. Accurate segmentation (boundary mapping) has been obtained from a class of chromosome spread images having variability in shape, size and other image properties using DCT based GVF active contours.

The characterization of the boundary mapping technique using DCT based GVF active contours has yielded[1] a set of parameter values that can be applied to obtain good boundary mapping in similar class of chromosome spread images. Standardization of the parameters is attempted by applying the same set of parameter values yielded by characterization study to a different dataset of chromosome spread images so that the standardization establishes that the parameters are independent of dataset and are truly standardized.

ACTIVE CONTOUR MODELS

Active contour or deformable curve is a high level boundary mapping technique based on curve evolution method and is advantageous with reference to its ability to generate closed parametric curves from images. The incorporation of a smoothness constraint provides robustness to noise and spurious edges.

Active contours, first proposed by Kass *et al.*[2] are energy minimizing contours that apply information about the boundaries as part of an optimization procedure. They are generally initialized by automatic or manual process around the object of interest. The contour then deforms itself iteratively from its initial position in conformity with nearest dominant edge feature, by minimizing the energy composed of the Internal and External forces to converge to the boundary of the object of interest.

The Internal forces computed from within the Active contour enforce smoothness of the curve and external forces that are derived from the image help to drive the curve toward the desired features of interest during the course of the iterative process.

The energy minimization process can be viewed as a dynamic problem where the active contour model is governed by the laws of elasticity and lagrangian dynamics[3] and the model evolves until equilibrium of all forces is reached, which is equivalent to a minimum of the energy function. The energy function is thus minimized, making the model active.

Corresponding Author: A. Prabhu Britto, Center for Medical Electronics,
Department of Electronics and Communication Engineering,
Anna University, Chennai 600025, India

FORMULATION OF ACTIVE CONTOUR MODELS

An active contour model can be represented by a curve c, as a function of its arc length τ,

$$c(\tau) = \begin{pmatrix} x(\tau) \\ y(\tau) \end{pmatrix} \quad (1)$$

with $\tau = [0...1]$. To define a closed curve, c (0) is set to equal c (1). A discrete model can be expressed as an ordered set of n vertices as $v_i=(x_i,y_i)^T$ with $v=(v_1,..,v_n)$ The large number of vertices required to achieve any predetermined accuracy could lead to high computational complexity and numerical instability[3].

Mathematically, an active contour model can be defined in discrete form as a curve x(s) = [x(s), y(s)], sε[0,1] that moves through the spatial domain of an image to minimize the energy functional

$$E = \int_0^1 \frac{1}{2}(\alpha|x'(s)|^2 + \beta|x''(s)|^2) + E_{ext}(x(s))^{ds} \quad (2)$$

where, α and β are weighting parameters that control the active contour's tension and rigidity, respectively[4].

The first order derivative discourages stretching while the second order derivative discourages bending. The weighting parameters of tension and rigidity govern the effect of the derivatives on the snake.

The external energy function E_{ext} is derived from the image so that it takes on smaller values at the features of interest such as boundaries and guides the active contour towards the boundaries. The external energy is defined by

$$E_{ext} = \kappa|G_\sigma(x,y) \times I(x,y)| \quad (3)$$

Where, G_σ (x,y) is a two-dimensional gaussian function with standard deviation σ, I (x,y) represents the image and κ is the external force weight. This external energy is specified for a line drawing (black on white) and positive κ is used.

A motivation for applying some gaussian filtering to the underlying image is to reduce noise. An active contour that minimizes E must satisfy the Euler Equation

$$\alpha x''(s) - \beta x''''(s) - \nabla E_{ext} = 0 \quad (4)$$

Where, $F_{int} = \alpha x''(s) - \beta x''''(s)$ and $F_{ext} = -\nabla E_{exi}$ comprise the components of a force balance equation such that

$$F_{int}+F_{ext}=0 \quad (5)$$

The internal force F_{int} discourages stretching and bending while the external potential force F_{ext} drives the active contour towards the desired image boundary.

Equation 4 is solved by making the active contour dynamic by treating x as a function of time t as well as s. Then the partial derivative of x with respect to t is then set equal to the left hand side of Eq. 4 as follows

$$x_t(s,t) = \alpha x''(s,t) - \beta x''''(s,t) - \nabla E_{ext} \quad (6)$$

A solution to Eq. 6 can be obtained by discretizing the equation and solving the discrete system iteratively[2]. When the solution x(s,t) stabilizes, the term x_t (s,t) vanishes and a solution of Eq. 4 is achieved.

Traditional active contour models suffer from a few drawbacks. Boundary concavities leave the contour split across the boundary. Capture range is also limited.

Methods suggested to overcome these difficulties, namely multiresolution methods[5], pressure forces[6], distance potentials[7], control points[8], domain adaptivity[9], directional attractions[10] and solenoidal fields[11], however solved one problem but introduced new ones[12]. Hence, a new class of external fields called gradient vector flow fields[12,13] was suggested to overcome the difficulties in traditional active contour models.

GRADIENT VECTOR FLOW (GVF) ACTIVE CONTOURS

Gradient Vector Flow (GVF) active contours use gradient vector flow fields obtained by solving a vector diffusion equation that diffuses the gradient vectors of a gray-level edge map computed from the image. The GVF active contour model cannot be written as the negative gradient of a potential function. Hence it is directly specified from a dynamic force equation, instead of the standard energy minimization network.

The external forces arising out of GVF fields are non-conservative forces as they cannot be written as gradients of scalar potential functions. The usage of non-conservative forces as external forces show improved performance of GVF field active contours compared to traditional energy minimizing active contours[12,13].

The GVF field points towards the object boundary when very near to the boundary, but varies smoothly over homogeneous image regions extending to the image border. Hence the GVF field can capture an active contour from long range from either side of the object boundary and can force it into the object boundary. The GVF active contour model thus has a large capture range and is insensitive to the initialization of the contour. Hence the contour initialization is flexible.

The gradient vectors are normal to the boundary surface but by combining laplacian and gradient the result

is not the normal vectors to the boundary surface. As a result of this, the GVF field yields vectors that point into boundary concavities so that the active contour is driven through the concavities. Information regarding whether the initial contour should expand or contract need not be given to the GVF active contour model. The GVF is very useful when there are boundary gaps, because it preserves the perceptual edge property of active contours[2,13].

The GVF field is defined as the equilibrium solution to the following vector diffusion equation[12],

$$u_t = g(|\nabla f|)\nabla^2 u - h(|\nabla f|)(u - \nabla f) \quad (7a)$$

$$u(x,0) = \nabla f(x) \quad (7b)$$

Where, u_t denotes the partial derivative of u(x,t) with respect to t, ∇^2 is the Laplacian operator (applied to each spatial component of u separately) and f is an edge map that has a higher value at the desired object boundary.

The functions in g and h control the amount of diffusion in GVF. In Eq. (7), $g(|\nabla f|\nabla^2 u)$ produces a smoothly varying vector field and hence called as the smoothing term, while $h(|\nabla f|$ (u-∇f) encourages the vector field u to be close to ∇f computed from the image data and hence called as the data term. The weighting functions $g(\cdot)$ and $h(\cdot)$ apply to the smoothing and data terms, respectively and they are chosen[13] as $g(|\nabla f|) = \mu$ and $h(|\nabla f|)=|\nabla f|^2$. $g(\cdot)$ is constant here and smoothing occurs everywhere, while $h(\cdot)$ grows larger near strong edges and dominates at boundaries.

Hence, the GVF field is defined as the vector field v(x,y)=[u(x,y),v(x,y)] that minimizes the energy functional

$$\varepsilon = \iint \mu(u_x^2 + u_y^2 + v_x^2 + v_y^2) + |\nabla f|^2 |v - \nabla f|^2 \, dxa \quad (8)$$

The effect of this variational formulation is that the result is made smooth when there is no data.

When the gradient of the edge map is large, it keeps the external field nearly equal to the gradient, but keeps field to be slowly varying in homogeneous regions where the gradient of the edge map is small, i.e., the gradient of an edge map ∇f has vectors point toward the edges, which are normal to the edges at the edges and have magnitudes only in the immediate vicinity of the edges and in homogeneous regions ∇f is nearly zero. μ is a regularization parameter that governs the tradeoff between the first and the second term in the integrand in Eq. 8. The solution of Eq. 8 can be done using the Calculus of Variations and further by treating u and v as functions of time, solving them as generalized diffusion equations[13].

DISCRETE COSINE TRANSFORM (DCT) BASED GVF ACTIVE CONTOURS

The transform of an Image yields more insight into the properties of the image. The Discrete Cosine Transform (DCT) has excellent energy compaction. Hence, the DCT promises better description of the image properties. The DCT is embedded into the GVF Active Contours. When the image property description is significantly low, this helps the contour model to give significantly better performance by utilizing the energy compaction property of the DCT.

The 2D DCT is defined as:

$$C(u,v) = \alpha(u)\alpha(v)\sum_{x=0}^{N-1}\sum_{y=0}^{N-1} f(x,y)\cos\left[\frac{(2x+1)u\pi}{2N}\right]\cos\left[\frac{(2Y+1)v\pi}{2N}\right] \quad (11)$$

The local contrast of the Image at the given pixel location (k,l) is given by

$$P(k,l) = \frac{\sum_{t=1}^{2(2n+1)-1} w_t E_t}{d_{00}} \quad (12)$$

where,

$$E_t = \frac{\sum_{u+v=t} |d_{u,v}|}{N} \quad (13)$$

and

$$N = \begin{cases} t+1 & t<2n+1 \\ 2(2n+1)t & t \geq 2n+1 \end{cases} \quad (14)$$

Here, w_t denotes the weights used to select the DCT coefficients. The local contrast P(k,l) is then used to generate a DCT contrast enhanced Image[14], which is then subject to selective segmentation by the energy compact gradient vector flow active contour model using Eq. 8.

MATERIALS AND METHODS

The chromosome metaphase image (at 72 pixels per inch resolution) provided by Prof. Ken Castleman and Prof. Qiang Wu (Advanced Digital Imaging Research, Texas) was taken and preprocessed. Insignificant and unnecessary regions in the image were removed interactively.

Interactive selection of the chromosome of interest was done by selecting a few points around the chromosome that formed the vertices of a polygon. On constructing the perimeter of the polygon, seed points for the initial contour were determined automatically by periodically selecting every third pixel along the perimeter of the polygon.

The GVF deformable curve was then allowed to deform until it converged to the chromosome boundary. The optimum parameters for the deformable curve with respect to the Chromosome images were determined by tabulated studies.

The image was made to undergo minimal preprocessing so as to achieve the goal of boundary mapping in chromosome images with very weak edges.

The DCT based GVF Active contour is governed by the following parameters, namely, F, µ, ", $ and 6. F determines the gaussian filtering that is applied to the image to generate the external field.

Larger value of F will cause the boundaries to become blurry and distorted and can also cause a shift in the boundary location. However, large values of F are necessary to increase the capture range of the active contour. µ is a regularization parameter in Eq. 8 and requires a higher value in the presence of noise in the image. " determines the tension of the active contour and $ determines the rigidity of the contour. The tension keeps the active contour contracted and the rigidity keeps it smooth. " and $ may also take on value zero implying that the influence of the respective tension and rigidity terms in the diffusion equation is low. 6 is the external force weight that determines the strength of the external field that is applied. The iterations were set suitably.

RESULTS AND DISCUSSION

DCT based GVF active contours were used to boundary map chromosome images from chromosome spread images. A few chromosome image samples, their corresponding DCT based GVF vector fields and their boundary mapped output images are presented here in Fig. 1 to 6 .

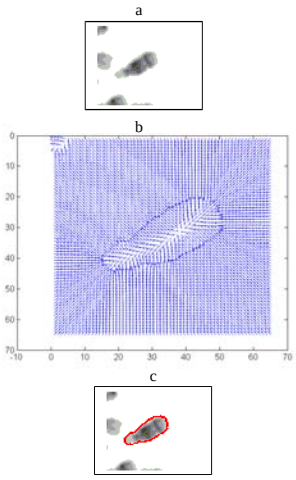

Fig. 1(a-c): a: Sample 1, b: Vector field 1, c: Output image 1

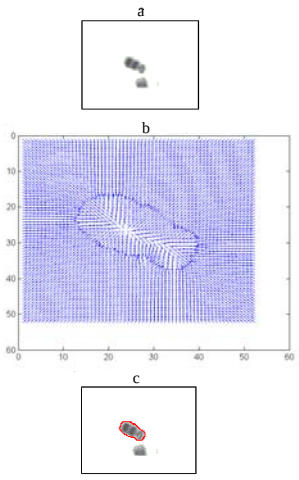

Fig. 2(a-c): a: Sample 2, b: Vector field 2, c: Output image 2

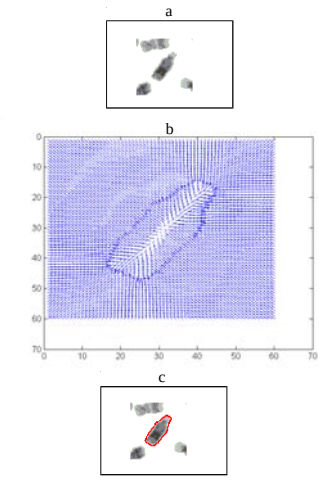

Fig. 3(a-c): a: Sample 3, b: Vector field 3, c: Output image 3

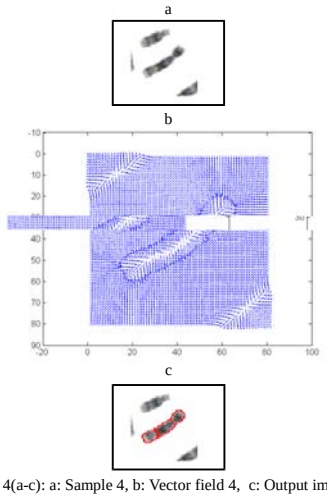

Fig. 4(a-c): a: Sample 4, b: Vector field 4, c: Output image 4

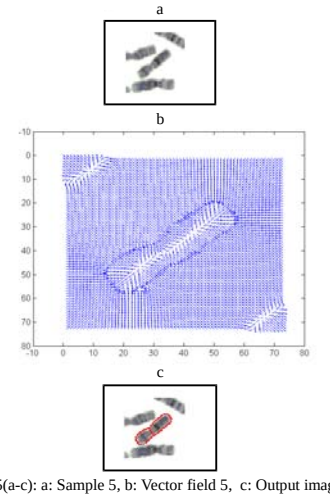

Fig. 5(a-c): a: Sample 5, b: Vector field 5, c: Output image 5

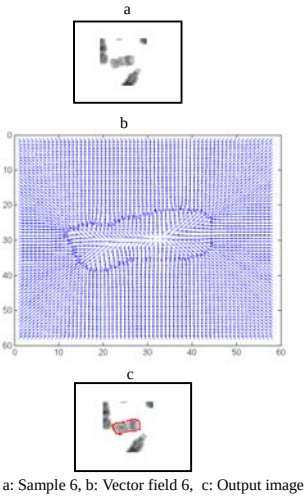

Fig. 6(a-c): a: Sample 6, b: Vector field 6, c: Output image 6

Fig. 1-6: Original chromosome image samples, their corresponding DCT based GVF fields and boundary mapped chromosome images as output images. (a) shows an original chromosome image sample, (b) shows its corresponding Vector Field and (c) shows its boundary mapped output image and henceforth

Figures above show successful boundary mapping of chromosome images using DCT based GVF Active Contours.

VALIDATION OF CHARACTERIZATION EXPERIMENTS

In order to quantify the performance of a segmentation method, validation experiments are necessary. Validation is typically performed using one or two different types of truth models. In this work, ground truth model is not available and hence validation is performed on ordinal or ranking scale and then quantified. A set of 10 random samples is taken and characterization of each parameter is done. The outputs were tabulated in ranking order with 1 describing the best quality output and as the quality decreases the rank increases up to rank 97. Rank 98 is a special case, where, the output image is rejected based on quality or the output image is not available due to numerical instability possibly caused due to the greater number of contour points[3]. The tables represent characterization studies for each parameter.

Each Table (1-6) denotes variation for only one parameter either between the lower and upper limits of the parameter or between the lower and upper limits giving significantly different output, with the other parameters taking a constant value. Hence, the best parameter value of that table is the one that gives maximum good quality outputs for all samples or a majority of samples and exhaustive study on every parameter is done by treating the other parameters as constants.

The statistical median is used to judge the distribution of values for each parameter value for all samples. When the median leans towards the lower values, i.e., towards 1, it indicates that almost 50% of the outputs lean towards 1, making that particular parameter value an optimal one and that optimal value is chosen.

The characterization studies reveal that each parameter sometimes has an optimal range within which it can assume any value thereby giving majority good outputs for all samples. But for the sake of experimental purposes, only the investigated discrete value of each parameter that gave best output was chosen.

An important point to be noted is that characterization studies have been performed for those parameter values which give either significant output or significant difference in performance between adjacent parameter values. Those parameter values where there is no significant difference between adjacent parameter values have not been tabulated. Also, those parameter values outside the tabulated range which gave no proper results have not been tabulated.

Table 1: Characterization of Sigma

	GVF (DCT) σ									
Sample No.	0.05	0.1	0.15	0.2	0.25	0.5	0.6	0.8	1	1.2
1	77	77	77	77	77	29	77	29	13	77
2	77	77	77	29	13	13	13	13	29	77
3	97	77	34	29	77	29	78	81	75	78
4	77	77	29	29	31	70	79	79	79	78
5	97	97	97	97	98	98	98	98	98	98
6	86	86	46	38	38	14	38	38	46	78
7	97	97	97	97	98	98	98	98	98	98
8	86	86	86	54	98	98	98	98	98	98
9	77	77	77	77	38	46	15	77	13	79
10	86	77	13	77	46	65	78	13	78	77
Median	86	77	77	66	62	55	78	78	77	78

Table 2: Characterization of Mu

	GVF (DCT) μ					
Sample No.	0.05	0.075	0.09375	0.1125	0.15	0.3
1	23	21	21	23	23	97
2	21	5	23	23	23	97
3	30	29	29	46	50	97
4	23	23	23	40	23	97
5	98	98	98	97	97	97
6	48	40	48	48	46	97
7	98	98	50	50	34	97
8	98	89	62	97	97	97
9	71	86	30	71	71	97
10	23	21	29	71	23	97
Median	39	35	29	49	40	97

Table 3: Characterization of Alpha

	GVF (DCT) α				
Sample No.	0	0.125	0.25	0.5	1
1	7	23	77	71	77
2	7	30	29	77	30
3	5	67	78	78	67
4	23	23	79	80	80
5	98	98	98	98	97
6	98	48	40	46	87
7	98	98	98	97	97
8	90	86	62	97	94
9	21	23	23	71	27
10	5	7	23	21	71
Median	22	39	70	78	79

The median indicates that the acceptable optimal range of σ is 0.2 to 0.5. The best value compared qualitatively amongst those tested is 0.25 and hence it is chosen for performing further characterization (Table 1).

The median indicates that the acceptable optimal range of μ is 0.05 to 0.09375. The best value compared qualitatively amongst those tested is 0.075 and hence it is chosen for performing further characterization (Table 2).

The median indicates that the acceptable optimal range of α extends from 0 to 0.125. The best value compared qualitatively amongst those tested is 0 and hence it is chosen for performing further characterization (Table 3).

The median indicates that the acceptable optimal range of β extends from 0 to 0.5. The best value compared

Table 4: Characterization of Beta

	GVF (DCT) β		
Sample No.	0	0.5	1
1	23	30	71
2	5	21	21
3	5	21	31
4	21	23	71
5	98	98	98
6	98	46	70
7	98	98	98
8	38	94	13
9	23	71	71
10	3	21	30
Median	23	38	71

Table 5: Characterization of Kappa

	GVF (DCT) κ					
Sample No.	0	0.5	0.625	0.75	0.875	1
1	97	7	5	5	5	5
2	97	3	3	3	1	1
3	97	21	19	21	30	67
4	97	7	7	7	23	71
5	97	98	98	98	98	98
6	97	98	98	98	86	98
7	97	98	98	98	98	98
8	97	86	98	97	98	82
9	97	7	7	23	23	21
10	97	21	5	19	19	21
Median	97	21	13	22	26	69

Table 6: Optimal range of DCT based GVF active contour parameter values for similar chromosome spread images

Parameters	Parameter value used for tested spread image	Acceptable range of parameter values	Acceptable range of parameter values at 5% tolerance
GVF (DCT) σ	0.25	[0.2, 0.5]	[0.1900, 0.5250]
GVF (DCT) μ	0.075	[0.05, 0.09375]	[0.0475, 0.0984]
GVF (DCT) α	0	[0, 0.125]	[0.0000, 0.1313]
GVF (DCT) β	0	[0, 0.5]	[0.0000, 0.5250]
GVF (DCT) κ	0.625	[0.5, 0.875]	[0.4750, 0.9187]

qualitatively amongst those tested is 0 and hence it is chosen for performing further characterization (Table 4).

The median indicates that the acceptable optimal range of κ extends from 0.5 to 0.875. The best value compared qualitatively amongst those tested is 0.625 (Table 5).

Hence the optimal set of parameter values that give good boundary mapping for the given class of chromosome images is σ = 0.25, μ = 0.075, α = 0, β = 0 and κ = 0.625. A safe limit of 5% tolerance can be introduced to the optimal range of parameter values to make them suitable for use in similar classes of chromosome spread images (Table 6).

In Table 6, values of acceptable range of parameters that can be used for successful boundary mapping similar classes of chromosome spread images are given.

STATISTICAL VALIDATION OF CHARACTERIZATION EXPERIMENTS

The parameters act independently on the boundary mapping scheme. In each characterization, the effect of other parameters will also be felt as they assume a definite constant value. In the course of the characterization study, optimum values for the respective parameters are chosen and applied as constant in the characterization study of the next parameter in the successive Table. In the last characterization study shown in Table 5, the values of σ, μ, α and β take on the chosen optimal values and only κ is investigated, thereby yielding a one way variation. Hence, one way analysis of variance on Table 5 is sufficient to test the significance of the entire boundary mapping process. A significant outcome from Table 5 will justify that the experimental results of Table 5 are valid, implying that the selected parameter values used as constants in Table 5 are also valid.

Hence, one way ANOVA test is performed on the last characterization (Table 5) to judge the experimental results. At the customary .05 significance level, one way Anova test yields a p value of 7.17082E-08 on Table 5[1], which rejects the null hypothesis. The very small p-value of 7.17082E-08 indicates that differences between the column means are highly significant. The probability of this outcome under the null hypothesis is less than 8 in 100,000,000. The test therefore strongly supports the alternate hypothesis that one or more of the samples are drawn from populations with different means. This implies that the results in Table 5 do not arise out of mere fluctuations and that the results are actually significant. Therefore, the experimental results are valid. This justifies that a suitable value of parameter κ can be chosen from Table 5 and that the constant values of parameters σ, μ, α and β used are also valid as these values also have significant influence on the results tabulated in Table 5.

Therefore, the experimental results and the inferences are also significant. The very small error in boundary mapping[1] substantiates that the characterized parameters have yielded very good segmentation results.

STANDARDIZATION

Characterization studies have yielded an acceptable optimal range of values for the parameters σ, μ, α, β and κ. To establish that the parameter values are standardized with reference to similar classes of chromosome spread images, standardization experiments are carried out in a similar class of chromosome spread images from a different dataset, made available by the kind courtesy of Dr.Michael Difilippantonio, Staff Scientist at the Section

Fig.7: Boundary mapped sample1

Fig. 8: Boundary mapped sample2

Fig. 9: Boundary mapped sample3

Fig. 10: Boundary mapped sample4

Fig. 11: Boundary mapped sample5

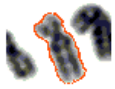

Fig. 12: Boundary mapped sample6

Fig. 13: Boundary mapped sample7

Fig. 14: Boundary mapped sample8

Fig. 15: Boundary mapped sample9

Fig. 16: Boundary mapped sample10

Fig. 17: Boundary mapped sample11

Fig. 18: Boundary mapped sample12

Fig. 19: Boundary mapped sample13

Fig. 20: Boundary mapped sample14

Fig. 21: Boundary mapped sample15

Fig. 22: Boundary mapped **sample16**

Fig. 23: Boundary mapped **sample17**

Fig. 24: Boundary mapped sa**mple18**

Fig. 25: Boundary mapped **sample19**

Fig. 26: Boundary mapped **sample20**

Fig. 27: Boundary mapped sam**ple21**

Fig. 28: Boundary mapped **sample22**

Fig.29: Boundary mapped s**ample23**

Fig. 30: Boundary mapped sampl**e24**

Fig. 31: Boundary mapped **sample25**

Fig. 32 Boundary mapped s**ample26**

Fig. 33: Boundary mapped sampl**e27**

Fig. 34: Boundary mapped sample28

Fig. 35: Boundary mapped sample29

Fig. 36: Boundary mapped sample30

Fig. 37: Boundary mapped sample31

Fig. 38: Boundary mapped sample32

Fig. 39: Boundary mapped sample33

Fig. 40: Boundary mapped sample34

Fig. 41: Boundary mapped sample35

Fig. 42: Boundary mapped sample36

Fig. 43: Boundary mapped sample37

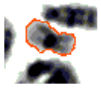

Fig. 44: Boundary mapped sample38

Fig. 45: Boundary mapped sample39

Fig. 46: Boundary mapped sample40

Fig. 47: Boundary mapped sample41

Fig. 48: Boundary mapped sample42

Fig. 49: Boundary mapped sample43

Fig. 50: Boundary mapped sample44

Fig. 51: Boundary mapped sample45

Fig. 52: Boundary mapped sample46

Fig. 53: Boundary mapped sample47

Fig. 54: Boundary mapped sample48

Fig. 55: Boundary mapped sample49

Fig. 56: Boundary mapped sample50

Fig. 57: Boundary mapped sample51

Fig. 58: Boundary mapped sample52

Fig. 59: Boundary mapped sample53

Fig. 60: Boundary mapped sample54

Fig. 61: Boundary mapped sample55

Fig. 62: Boundary mapped sample56

Fig. 63: Boundary mapped sample57

Fig. 64: Boundary mapped sample58

Fig. 65: Boundary mapped sample59

Fig. 66: Boundary mapped sample60

Fig. 67: Boundary mapped sample61

Fig. 68: Boundary mapped sample62

Fig. 69: Boundary mapped sample63

Fig. 70: Boundary mapped sample64

Fig. 71: Boundary mapped sample65

Fig. 72: Boundary mapped sample66

Fig. 73: Boundary mapped sample67

Fig. 74: Boundary mapped sample68

Fig. 75: Boundary mapped sample69

Fig. 76: Boundary mapped sample70

Fig. 77: Boundary mapped sample71

Fig. 78: Boundary mapped sample72

Fig. 79: Boundary mapped sample73

Fig. 80: Boundary mapped sample74

Fig. 81: Boundary mapped sample75

Fig. 82: Boundary mapped sample76

Fig. 83: Boundary mapped sample77

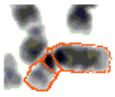

Fig. 84: Boundary mapped sample78

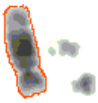

Fig. 85: Boundary mapped sample79

Fig. 86: Boundary mapped sample80

Fig. 87: Boundary mapped sample81

Fig. 88: Boundary mapped sample82

Fig. 89: Boundary mapped sample83

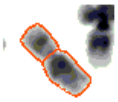

Fig. 90: Boundary mapped sample84

Fig. 91: Boundary mapped sample85

Fig. 92: Boundary mapped sample86

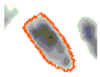

Fig. 93: Boundary mapped sample87

Fig. 94: Boundary mapped sample88

Fig. 95: Boundary mapped sample89

Fig. 96: Boundary mapped sample90

Fig. 97: Boundary mapped sample91

Fig. 98: Boundary mapped sample92

Fig. 99: Boundary mapped sample93

Fig. 100: Boundary mapped sample94

Fig. 101: Boundary mapped sample95

Fig. 102: Boundary mapped sample96

Fig.103: Boundary mapped sample97

Fig.104: Boundary mapped sample98

Fig. 105: Boundary mapped sample99

Fig.106: Boundary mapped sample100

Fig. 107: Boundary mapped sample101

Fig. 108: Boundary mapped sample102

Fig.109: Boundary mapped sample103

Fig. 110: Boundary mapped sample104

Fig. 111: Boundary mapped sample105

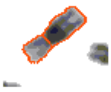

Fig. 112: Boundary mapped sample106

Fig. 113: Boundary mapped sample107

Fig. 114: Boundary mapped sample108

Fig. 115: Boundary mapped sample109

Fig. 116: Boundary mapped sample110

Fig. 117: Boundary mapped sample111

Fig.118: Boundary mapped sample112

Fig.119: Boundary mapped sample113

Fig. 120: Boundary mapped sample114

Fig.121: Boundary mapped sample115

Fig.122: Boundary mapped sample116

Fig. 123: Boundary mapped sample117

Fig.124: Boundary mapped sample118

Fig.125: Boundary mapped sample119

Fig. 126: Boundary mapped sample120

Fig.127: Boundary mapped sample121

Fig.128: Boundary mapped sample122

Fig. 129: Boundary mapped sample123

Fig.130: Boundary mapped sample124

Fig. 131: Boundary mapped sample125

Fig. 132: Boundary mapped sample126

Fig.133: Boundary mapped sample127

Fig. 134: Boundary mapped sample128

Fig. 135: Boundary mapped sample129

Fig.136: Boundary mapped sample130

Fig. 137: Boundary mapped sample131

Fig. 138: Boundary mapped sample132

Fig.139: Boundary mapped sample133

Fig.140: Boundary mapped sample134

Fig. 141: Boundary mapped sample135

Fig.142: Boundary mapped sample136

Fig. 143: Boundary mapped sample137

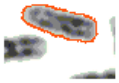

Fig. 144: Boundary mapped sample138

Fig. 145: Boundary mapped sample139

Fig. 146: Boundary mapped sample140

Fig.147: Boundary mapped sample141

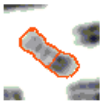

Fig.148: Boundary mapped sample142

Fig. 149: Boundary mapped sample143

Fig. 150: Boundary mapped sample144

Fig.151: Boundary Mapped Sample145

Fig.152: Boundary Mapped Sample146

Fig.153: Boundary Mapped Sample147

Fig.154: Boundary mapped sample148

Fig. 155: Boundary mapped sample149

Fig. 156: Boundary mapped sample150

of Cancer Genomics, Genetics Branch/CCR/NCI/NIH, Bethesda MD. Therefore, the standardization experiments are expected to establish that the set of characterized parameters[1] give good boundary mapping results in chromosome spread images, independent of the dataset from which the chromosome spread images are obtained and are thus truly standardized.

The same characterized parameter values[1] that have given very small boundary mapping error have been used, viz., $\sigma = 0.25$, $\mu = 0.075$, $\alpha = 0$, $\beta = 0$ and $\kappa = 0.625$. Very good boundary mapping results have been obtained on the new dataset and the results are shown in the following pages. Each sample is unique as the chromosomes are imaged in a fluid medium and random bending effects are manifested. Hence it is shown that the DCT based GVF Active Contour, governed by the characterized values of the parameters of $\sigma = 0.25$, $\mu = 0.075$, $\alpha = 0$, $\beta = 0$ and $\kappa = 0.625$ are able to overcome the variations in the shape of the chromosomes and give good boundary mapping in each of the samples independent of the dataset.

A few samples from another dataset are used for standardizing the boundary mapping technique and the results are illustrated in the following pages. The chromosome image is seen in gray scale, while the DCT based GVF Active Contour mapped boundary is shown in red.

Figure 7-156 show boundary mapped chromosomes and establish that the boundary mapping process has been very successfully accomplished accurately. The above dataset of chromosome spread images used for testing standardization is different from the dataset of chromosome spread images used for characterization. It is hence found that the characterized parameters are thus able to accomplish successfully accurate segmentation in a different dataset also. Therefore the characterized parameters have now become standardized and accomplish good boundary mapping independent of dataset from which the images are obtained.

Hence, it is inferred that the set of parameter values $\sigma = 0.25$, $\mu = 0.075$, $\alpha = 0$, $\beta = 0$ and $\kappa = 0.625$ governing the formulation of the DCT based GVF Active Contours are hence standardized and these parameter vales can be applied to obtain successful boundary mapping in similar classes of chromosome spread images, independent of the dataset from which they are obtained.

CONCLUSION

The discrete cosine transform based gradient vector flow active contours can therefore, be used as a standardized tool for successful boundary mapping of chromosome spread images, independent of the dataset from which they are obtained.

The values $\sigma = 0.25$, $\mu = 0.075$, $\alpha = 0$, $\beta = 0$ and $\kappa = 0.625$ have hence been standardized and can be used for accurate boundary mapping of similar classes of chromosome spread images using DCT based GVF active contours.

ACKNOWLEDGEMENTS

The authors express their thanks to Dr. Michael Difilippantonio, Staff Scientist at the Section of Cancer Genomics, Genetics Branch/ CCR / NCI / NIH, Bethesda MD and Prof. Ken Castleman and Prof. Qiang Wu, from Advanced Digital Imaging Research, Texas for their help in providing chromosome images.

REFERENCES

1. Britto, A.P. and G. Ravindran, 2005. Boundary mapping of chromosome spread images using optimal set of parameter values in discrete cosine transform based gradient vector flow active contours. J. Applied Sci., (accepted, in print)
2. Kass, M., A. Witkin and D. Terzopoulos, 1987. Snakes: Active contour models, Intl. J. Comp. Vision 1: 321-331.
3. Rueckert, D., 1997. Segmentation and tracking in cardiovascular MR images using geometrically deformable models and templates. Ph.D Thesis, Imperial College of Science, Technology and Medicine, London.
4. Xu, C. and J.L. Prince, 1997. Gradient Vector Flow: A new external force for snakes. IEEE Proceedings of Conference on Computer Vision and Pattern Recognition (CVPR'97), pp: 66-71.
5. Leroy, B., I. Herlin and L.D. Cohen, 1996. Multi-resolution algorithms for active contour models. In: 12th Intl. Conf. Analysis and Optimization of Systems, pp: 58-65.
6. Cohen, L.D., 1991. On active contours and balloons, CVGIP: Image Understanding, 53: 211-218.
7. Cohen, L.D. and I. Cohen, 1993. Finite-element methods for active contour models and balloons for 2-D and 3-D images, IEEE Transactions on Pattern Analysis and Machine Intelligence, 15: 1131-1147.
8. Davatzikos, C. and J.L. Prince, 1995. An active contour model for mapping the cortex. IEEE Trans. Medical Imaging, 14: 65-80.
9. Davatzikos, C. and J.L. Prince, 1994. Convexity analysis of active contour models. In: Proc. Conf. Info. Sci. Sys., pp: 581-587.

10. Abrantes, A.J. and J.S. Marques, 1996. A class of constrained clustering algorithms for object boundary extraction. IEEE Transactions on Image Processing, 5:1507-1521.
11. Prince, J.L. and C.Xu, 1996. A new external force model for snakes, In: 1996 Image and Multidimensional Signal Processing Workshop, pp: 30-31.
12. Xu, C. and J.L. Prince, 2000. Gradient Vector Flow Deformable Models. In Handbook of Medical Imaging, Academic Press, pp: 159-169.
13. Xu, C. and J.L. Prince, 1998. Snakes, shapes and gradient vector flow, IEEE Transactions on Image Processing, 7: 359-369.
14. Jinshan, T. and S.T. Acton, 2004. A DCT based gradient vector flow snake for object boundary detection. 6th IEEE Southwest Symposium on Image Analysis and Interpretation, pp: 157-161.